Mathematical Biosciences 363 (2023) 109052

Contents lists available at ScienceDirect

Mathematical Biosciences

journal homepage: www.elsevier.com/locate/mbs

Original Research Article

The role of Type I interferons in the pathogenesis of foot-and-mouth disease virus in cattle: A mathematical modelling analysis

Kyriaki Giorgakoudi [a,b,*,1], David Schley [a,2], Nicholas Juleff [a,3], Simon Gubbins [a,4], John Ward [b,4]

[a] The Pirbright Institute, Ash Road, Pirbright, Surrey, GU24 0NF, UK
[b] Department of Mathematical Sciences, Loughborough University, Loughborough, Leicestershire, LE11 3TU, UK

ARTICLE INFO

Keywords:
Interferon
Cytokines
Infection
Foot-and-mouth disease virus
Mathematical model
Cell death

ABSTRACT

Type I interferons (IFN) are the first line of immune response against infection. In this study, we explore the interaction between Type I IFN and foot-and-mouth disease virus (FMDV), focusing on the effect of this interaction on epithelial cell death. While several mathematical models have explored the interaction between interferon and viruses at a systemic level, with most of the work undertaken on influenza and hepatitis C, these cannot investigate why a virus such as FMDV causes extensive cell death in some epithelial tissues leading to the development of lesions, while other infected epithelial tissues exhibit negligible cell death. Our study shows how a model that includes epithelial tissue structure can explain the development of lesions in some tissues and their absence in others. Furthermore, we show how the site of viral entry in an epithelial tissue, the viral replication rate, IFN production, suppression of viral replication by IFN and IFN release by live cells, all have a major impact on results.

1. Introduction

Type I interferon (IFN) are regulatory proteins belonging to the superfamily of cytokines. In the event of an infection, they are the host's first line of defence. They do this by binding to cell surface receptors and activating intracellular signalling pathways. This leads to protein synthesis [1] that can stimulate antiviral action such as suppression of viral replication [2,3] and inhibition of cell infection [4].

Understanding the interplay between pathogens and Type I IFN is important: it can be a crucial step towards identifying ways to mitigate disease. For FMDV, a Picornavirus infecting cloven-hoofed animals, understanding the FMDV-host interaction and the way FMDV evades innate immune response has a role to play in developing effective disease control strategies [5].

An open question in FMDV pathogenesis is the development of vesicular lesions and their localisation [6]. Lesions are the result of extensive epithelial cell death following infection and they can be found in the epithelial tissues of the tongue, snout, coronary band and mammary glands. What we do know about FMDV and epithelial cells is that, similarly to other viruses, it induces local IFN production. This helps neighbouring cells to prepare ahead of viraemia [5]. If viraemia does occur then plasmacytoid dendritic cells can produce up to 1000-fold more IFN than other cells [1,7] while defending the host.

While there are many mathematical models on virus-IFN dynamics, there has been little work carried out at tissue level [8] and none – to our knowledge – on tissue level FMDV-IFN dynamics. FMDV-IFN dynamics have been modelled at whole animal (cow) level by Howey et al. [9]. The authors combined in vivo experimental work with an eight compartments ODE model, where both innate and adaptive immune response were included. Type I IFN and antibodies were both shown to determine the peak levels of FMDV in the animal.

Mathematical models of influenza [10,11] and hepatitis C [12–14] have explored virus-IFN dynamics. Interaction of cytokines and viruses has also been explored in relation to dengue [15], Newcastle disease [16] and Herpes simplex type 1 [8] models.

The model of Baccam et al. [17] showed cells' average lifetime to be shorter than experimental values. This led authors to hypothesise that IFN action could inhibit viral production while maintaining cells alive. Hancioglu et al. [18] assumed that IFNs could make cells infection-resistant. Both explored influenza dynamics in human respiratory epithelial cells. Other influenza models explored IFN action in

* Corresponding author.
E-mail addresses: K.Giorgakoudi@city.ac.uk (K. Giorgakoudi), David@senseaboutscience.org (D. Schley), nick.juleff@gatesfoundation.org (N. Juleff), simon.gubbins@pirbright.ac.uk (S. Gubbins), john.ward@lboro.ac.uk (J. Ward).
[1] Present addresses: Department of Health Services Research and Management, School of Health Sciences, City, University of London, UK; NIHR Biomedical Research Centre at The Royal Marsden NHS Foundation Trust and The Institute of Cancer Research, UK
[2] Present address: Sense about Science, UK.
[3] Present address: Bill & Melinda Gates Foundation, Seattle Washington, US.
[4] Joint senior authors.

https://doi.org/10.1016/j.mbs.2023.109052
Received 27 January 2023; Received in revised form 16 June 2023; Accepted 18 July 2023
Available online 24 July 2023

mice [19], ferrets [20], chickens [21] and horses [22]. Cao et al. [20] showed with their models how IFN-induced inhibition of viral production can explain dynamics that IFN-induced cell resistance alone cannot. Hernandez-Vargas et al. [19] suggested that higher IFN levels in the elderly lead to slower viral growth, impaired immune response and hindered viral clearance. The model of Saenz et al. [22] suggested that cell death and cell damage are a result of both high IFN production and poor IFN efficiency in protecting cells from infection. Xie et al. [21] highlighted the crucial importance of Type I IFN in the absence of adaptive immune response.

Neumann et al. [12] developed a model of Hepatitis C virus (HCV) infection, where they explored the effect of different Type I IFN dose regimens on infected individuals. They showed that IFN inhibits viral production and release. Sasmal et al. [15] showed cytokines to be important in the clearance of dengue virus. In contrast to the ordinary differential equation models used in most studies, Howat et al. [8] formed an individual-based, spatial stochastic model to investigate Herpes simplex virus 1 interaction with IFN. Their model suggested that where epithelial cells cannot fight infection, they may act as IFN producers to protect other areas.

More recently, Wang et al. [23] used a combination of differential equations and stochastic modelling to explore COVID-19 infection dynamics. Their results have highlighted that Type I IFN production can delay the development of clinical symptoms. Another model of COVID-19 infection has showed IFN in combination with antiviral drugs to reduce the time to recovery [24]. Sadria and Layton [25] modelled the dynamics of COVID-19 infection including both innate and adaptive immune response. Their model shows IFN response to peak alongside the viral load, with remaining cells becoming resistant to infection.

In this study, we investigated the interplay between FMDV and Type I IFN, the resulting epithelial cell death and localisation of vesicular lesions. FMDV-induced epithelial cell death has been previously explored by other models [26,27], with the latter indicating that inhibition of FMDV growth could play an important role in the localisation of lesions and suggested the exploration of IFN antiviral action [27]. Here we have introduced Type I IFN in a spatio-temporal partial differential equation (PDE) model. This is one of a few tissue-level models of virus-IFN interaction. We have compared the epithelial tissue of the tongue with that of the dorsal soft palate (DSP); the former exhibits extensive epithelial cell death while the latter presents no or negligible death in response to FMDV infection despite being a primary site of infection.

2. Materials and methods

The model is formulated to predict the spatio-temporal evolution of FMDV and cells across the epithelial layers; thereby being able to predict the extent of epithelium damage and where it is most likely to occur during the early stages of infection. Full details of the modelling are discussed in [27] and we will only summarise the common components here.

The timescale of interest is the first 48 h of infection, which is a timescale sufficient for the development of lesions [6] but before adaptive immunity begins to a play a significant role. The model epithelium structure is assumed to be governed by a diffusible generic growth factor (e.g. epithelial growth factor (EGF), concentration E) that is sourced at the base ($x = 0$) and is used up by live cells in the epithelium it diffuses into it. Differentiation of the epithelial cells is such that the basal cell layer corresponds to when $E > E_B$, spinal cells when $E_G < E < E_B$ and granular cells when $E < E_G$. The epithelial cell layer structure is presented in Fig. 1. Since we are only concerned with the dynamics in the first 48 h, negligible epithelial growth and regrowth is assumed [27], and only cell death occurs due to FMDV infection. Intracellular resource (K), represents the essential resources for cell function and survival that are depleted during FMDV replication, leading to cell lysis. Our model makes no distinction between apoptosis and necrosis due to the lack of information on the type of death leading to cell lysis in FMDV-infected tissues [28].

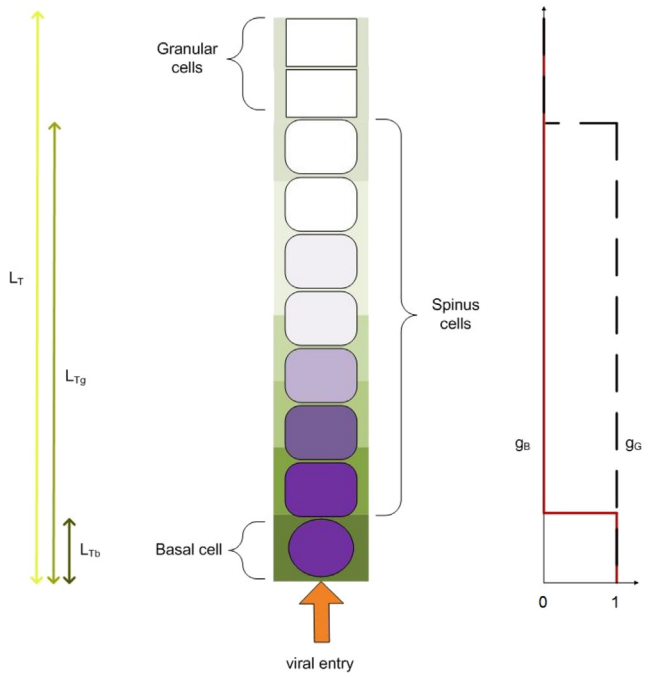

Fig. 1. Schematic showing the epithelial structure assumed in the mathematical modelling. Example of FMDV infection of tongue epithelial cells with virus entering through the basement membrane. Darker shades of green and purple indicate higher concentration of extracellular and cellular FMDV respectively. Infection dynamics are the same in DSP, though tissue structure and usual site of viral entry are different. Tongue epithelium thickness is L_T, basal-spinous epithelium thickness is L_{T_b}, while basal cell layer thickness is L_{T_b} (left hand side). For DSP the equivalents are L_P for epithelium thickness and L_{P_b} for basal cell layer thickness. No granular layer is present in DSP, therefore there is no distinction between whole epithelium and basal-spinous epithelium thickness. Function g_B (red line, right hand side) takes values of approximately 1 for basal cells, dropping to approximately zero everywhere else. Function g_G (black dashed line) is approximately 1 for the basal-spinous epithelium, dropping to approximately zero for granular cells. Figure and caption reproduced from [27] under the Creative Commons [CC BY] license.

Table 1
Model variables.

	Variable	Units
S_c	Cellular volume fraction	(non dimensional)
S_e	Extracellular volume fraction	(non dimensional)
V_c	Intracellular viral concentration	PFU $\times$ cm^{-1}
V_e	Extracellular viral concentration	PFU $\times$ cm^{-1}
I_c	Intracellular IFN concentration	cm^{-1}
I_e	Extracellular IFN concentration	cm^{-1}
K	Intracellular resource	cm^{-1}
E	Activator concentration	cm^{-1}

The health of the epithelial tissue can be assessed through variable $S_c(x,t)$, which represents the volume fraction of live cells ($S_e = 1 - S_c$ is the volume fraction of extracellular space). In a healthy state, $S_c(x,t)$ will be spatially uniform with a fraction set to α. Viral concentration is tracked in both the cellular and extracellular space (V_c and V_e respectively), as well as IFN concentration (I_c and I_e respectively). Model variables are presented in Table 1, while Tables 2 and 3 summarise model parameters. Initial and boundary conditions parameters are presented in Table 4, where at $t = 0$ the skin is assumed to be in a healthy, homoeostatic state.

2.1. Response functions

The epithelial tissue structure as described by the model is governed by the sigmoidal response functions $g_B(E) \in [0,1]$ and $g_G(E) \in [0,1]$ for $E \leq 0$. The basal cell (proliferating) layer corresponds to $g_B(E) \approx 1$

Table 2
Base parameter values for model parameters. Methods of estimation are provided in S2 Supplementary information or can be found in [27]. Parameters relating to the response functions are presented separately in Table 3.

	Parameter	Value
λ	Uptake rate of activator by cells	1.97×10^{-12} h^{-1} (based on [29], see [27])
δ	Decay rate of activator	0.693 h^{-1} (based on [30], see [27])
D_E	Diffusion coefficient of activator	1.86×10^{-3} cm^2 h^{-1} (based on [31], see [27])
Φ	Maximum rate of cell lysis due to viral infection	3.33×10^{-1} h^{-1} (based on [32], see [27])
Ψ	Maximum IFN-mediated infected cell death rate	0.416 h^{-1} (based on [32,33])
ξ	Maximal replication rate of virus	1.56×10^{-1} PFU/resource fraction (based on [34], see [27])
ρ	Rate at which virus uses up intracellular resource	2.46×10^{-2}/(PFU × h × cm^{-1} (based on [34], see [27])
μ	Virion-cell affinity and internalisation rate	2×10^{-5} h^{-1} (based on [35], see [27])
γ	Rate of virus release by live cells	0 h^{-1} [27]
D_V	Diffusion coefficient of virions	3.67×10^{-4} cm^2/ h ([36], see [27]
θ	Maximal hourly IFN production constant	5.13 h^{-1} (based on [37–39])
μ_I	IFN uptake by cells rate	1.4×10^{-5} h^{-1} (based on [40–44])
γ_I	IFN release rate by live cells	5.14×10^{-1} h^{-1} (based on [45])
δ_{I_c}	Intracellular IFN decay rate	5.59×10^{-2} h^{-1} (based on [46])
δ_{I_e}	Extracellular IFN decay rate	5.59×10^{-2} h^{-1} (based on [46])
D_I	IFN diffusion coefficient	2.95×10^{-3} cm^2/h (based on [8,47–50])
Q_I	IFN mass transfer coefficient	4.56×10^{-2} cm×h^{-1} (based on [8,27,31])
ϵ_1	IFN production term coefficient	1 IU/PFU (see S2 Supplementary Information)
ϵ_2	IFN production term coefficient	0.1 PFU/cm^{-1} (see S2 Supplementary Information)
ϵ_3	IFN production term coefficient	1 PFU/cm^{-1} (see S2 Supplementary Information)
ϵ_4	IFN production term coefficient	0.25 IU/cm^{-1} (see S2 Supplementary Information)
I_R	Intracellular IFN threshold for FMDV replication inhibition	0.45 IU/cm (see S2 Supplementary Information)
I_U	Intracellular IFN threshold for FMDV uptake by cells inhibition	(based on [4])
I_L	Intracellular IFN threshold for FMDV live cell release inhibition	0.45 IU/cm (see S2 Supplementary Information)
I_D	IFN threshold of IFN-mediated cell death	50 IU/cm (see S2 Supplementary Information)
V_D	FMDV threshold of IFN-mediated cell death	30 PFU/cm (see S2 Supplementary Information)
L_P	Thickness of dorsal soft palate	1.71×10^{-2} cm [27]
L_T	Thickness of tongue	1.66×10^{-1} cm [27]
L_{Pb}	Threshold of spinous cell layer in dorsal soft palate	1.41×10^{-3} cm [27]
L_{Tb}	Threshold of spinous cell layer in tongue	1.22×10^{-3} cm [27]
L_{Tg}	Threshold of granular cell layer in tongue	1.59×10^{-1} cm [27]

Table 3
Base parameter values for model parameters relating to response functions. Methods of estimation are provided in S2 Supplementary information or can be found in [27].

	Parameter	Value
E_B	Concentration of E at basal-spinous interface	9.66×10^{-1} cm^{-1} (DSP) [27], 9.77×10^{-1} cm^{-1} (tongue) [27]
E_G	Concentration of E at spinous-granular interface (DSP) or Spinous-surface interface (tongue)	6.3×10^{-1} (DSP) [27], 8.18×10^{-2} (tongue) [27]
m_2	Exponent in function g_B that defines the basal layer	80 [27]
m_3	Exponent in function g_G that defines the basal and spinous layers	80 [27]
$K_{1/2}$	Value of K at which cell death is half maximum value	38.1 resource units × cm^{-1} [27]
m_1	Exponent in function f that defines resource depletion	4 [27]
ρ_B	Defines relative vulnerability of basal layer to FMDV replication	1 [27]
ρ_S	Defines relative vulnerability of spinous layer to FMDV replication	1 [27]
μ_B	Defines relative vulnerability of basal layer to FMDV infection	1[27]
μ_S	Defines relative vulnerability of spinous layer to FMDV infection	1 [27]
ζ_B	Defines relative competence of basal layer to produce IFN	1 (see S2 Supplementary Information)
ζ_S	Defines relative competence of spinous layer to produce IFN	1 (see S2 Supplementary Information)
η_B	Defines relative competence of basal layer to uptake IFN	1 (see S2 Supplementary Information)
η_S	Defines relative competence of spinous layer to uptake IFN	1 (see S2 Supplementary Information)
m_4	Exponent in IFN component of function f_D	4 (see S2 Supplementary Information)
m_5	Exponent in FMDV component of function f_D	4 (see S2 Supplementary Information)
m_6	Exponent in function f_R that defines FMDV replication inhibition	2 (see S2 Supplementary Information)
m_7	Exponent in function f_U that defines FMDV uptake by cells inhibition	2 (see S2 Supplementary Information)
m_8	Exponent in function f_L that defines FMDV live cell release inhibition	2 (see S2 Supplementary Information)

Table 4
Initial and boundary conditions parameters.

	Parameter	Condition	Value
α	Initial cellular space volume	$S_c(x,0)$	0.95 [26]
E_0	Activator at the basement membrane	$E(0,t)$	1 cm^{-1}
K_0	Initial intracellular resource fraction per unit length	$K(x,0)$	952 cm^{-1}
V_0	Viral infectious dose	$V_e(e_p,0)$	2290 PFU × cm^{-1}
Q_E	Activator mass transfer coefficient	$\frac{\partial E}{\partial x}(L_P)$	5.69×10^{-2} cm × h^{-1}
Q_V	FMDV mass transfer coefficient	$\frac{\partial V_e}{\partial x}(L_P)$	2.85×10^{-2} cm × h^{-1}
e_p	Viral entry point	Various points tested	0, 3×10^{-3}cm, L_i or $L_i - 3 \times 10^{-3}$ cm, where $i = P, T$

Table of parameters of initial and boundary conditions. Estimates sourced from [27].

and for the spinus and granular cells $g_B(E) \approx 0$, whilst in the basal and spinus layers $g_G(E) \approx 1$ and for granular cells $g_G(E) \approx 0$. This is to distinguish between proliferating (basal) and non-proliferating cells (spinous and granular) [51], and cells where viral replication and uptake take place (basal and spinous) and cells where they do not (granular). The latter is an assumption based on the presence of FMDV and integrins associated with its uptake in basal and spinous layers in contrast with the granular layer [52,53]. The two functions are continuous to represent the unclear boundaries between layers. The functions used are

$$g_B(E) = \frac{E^{m_2}(E_0^{m_2} + E_B^{m_2})}{E_0^{m_2}(E^{m_2} + E_B^{m_2})} \tag{1}$$

$$g_G(E) = \frac{E^{m_3}(E_0^{m_3} + E_G^{m_3})}{E_0^{m_3}(E^{m_3} + E_G^{m_3})}, \tag{2}$$

where E_B is the threshold activator concentration defining the basal-spinous boundary, E_G defines the spinous-granular boundary (tongue) and spinous-epithelium surface (DSP), and E_0 is the concentration at $x = 0$. A schematic diagram of the values of g_B and g_G over the tongue and DSP epithelia can be found in Fig. 1.

Interlayer variability in FMDV replication is expressed by response functions $h_R(E)$ and $h_U(E)$. We have

$$h_R(E) = \rho_S + (\rho_B - \rho_S)g_B(E) \tag{3}$$

$$h_U(E) = \mu_S + (\mu_B - \mu_S)g_B(E), \tag{4}$$

where parameters ρ_B and ρ_S express cell vulnerability to FMDV replication (basal and spinous cells respectively), while μ_B and μ_S express cell vulnerability to FMDV infection (basal and spinous cells respectively). For example, if basal cells are assumed to be more vulnerable to infection, then $\mu_B > \mu_S$, etc.

The variable K represents a resource that is required for cell survival, but is consumed by virus in the replication process. The cells are assumed to die at a rate proportional to $f(K) \in [0, 1]$, such that if the resource is sufficiently depleted, i.e. $K < K_{1/2}$ then $f(K) \approx 1$; we thus assume

$$f(K) = \frac{{K_{1/2}}^{m_1}}{{K_{1/2}}^{m_1} + K^{m_1}}. \tag{5}$$

All of the above response functions are also presented in detail by Giorgakoudi et al. [27]. In this FMDV-IFN model, we have introduced a number of response functions describing interlayer variability and cell death in relation to IFN activity, which are presented below.

Interlayer variability of IFN production and IFN uptake by cells is controlled by functions $h_I(E)$ and $h_{I_U}(E)$ respectively. Both functions are constrained to be in $[0, 1]$, with $h_I(E) \simeq \zeta_S$ and $h_{I_U}(E) \simeq \eta_S$ in the spinous layer and $h_I(E) \simeq \zeta_B$ and $h_{I_U}(E) \simeq \eta_B$ in the basal layer. In the baseline scenario we assume equal IFN production and uptake competence by basal and spinous cells, however alternative scenarios will be investigated. If we were to assume higher IFN production in the basal layer then we would have $\zeta_B > \zeta_S$. The absolute difference between ζ_B and ζ_S is a measure of the difference in IFN production competence between basal and spinous cells. The same applies for parameters η_B and η_S, defining IFN uptake competence by basal and spinous layers respectively. Hence,

$$h_I(E) = \zeta_S + (\zeta_B - \zeta_S)g_B(E), \tag{6}$$

$$h_{I_U}(E) = \eta_S + (\eta_S - \eta_S)g_B(E). \tag{7}$$

IFN-mediated cell death is considered to affect only infected cells with high IFN concentration. The response function $f_D(I_c, V_c)$ the IFN mediated cell death rate in the presence of virus, relative to threshold parameters I_D and V_D. The functional form is assumed to be

$$f_D(I_c, V_c) = \frac{{I_c}^{m_4}}{{I_c}^{m_4} + {I_D}^{m_4}} \frac{{V_c}^{m_5}}{{V_c}^{m_5} + {V_D}^{m_5}}, \tag{8}$$

noting that $f_D(I_D, V_D) = \frac{1}{4}$.

To incorporate the inhibitory action of IFN towards FMDV replication, FMDV uptake by cells and FMDV release, we have incorporated a set of Hill-like response functions. These are f_R, f_U and f_L, regulating FMDV replication, FMDV uptake by cells and FMDV release by live cells respectively. In the absence of IFN these functions are equal to unity and thus do not influence FMDV activity. For $I_c \gg I_R$, where I_R is an IFN threshold in the f_R function, $f_R(I_c) \simeq 0$. IFN thresholds I_U and I_L regulate functions f_U and f_L respectively in a similar way. We define

$$f_R(I_c) = \frac{{I_R}^{m_6}}{{I_R}^{m_6} + {I_c}^{m_6}} \tag{9}$$

$$f_U(I_c) = \frac{{I_U}^{m_7}}{{I_U}^{m_7} + {I_c}^{m_7}} \tag{10}$$

$$f_L(I_c) = \frac{{I_L}^{m_8}}{{I_L}^{m_8} + {I_c}^{m_8}} \tag{11}$$

with equations punctuated.

2.2. Mathematical model

As in [27] the activator, E, equation defines the epithelial structure, thus

$$\underbrace{D_E \frac{\partial^2 E}{\partial x^2}}_{\text{activator diffusion}} - \underbrace{\lambda S_c E}_{\text{activator uptake by cells}} - \underbrace{\delta E}_{\text{activator decay}} = 0 \tag{12}$$

and the epithelial tissue consists of cellular and extracellular space, S_c and S_e respectively, hence

$$\underbrace{S_e(x,t)}_{\text{extracellular space fraction}} + \underbrace{S_c(x,t)}_{\text{cellular space fraction}} = 1. \tag{13}$$

Here, cell death is assumed to occur for two reasons; mainly because of FMDV replication inflicting damage to infected cells but also because of IFN-mediated cell death [33,54]. While other innate immune response components (e.g. macrophages, natural killer cells) will play a role in reducing viral load and inducing cell death, considering FMDV's ability to effectively evade innate immunity [5] we have only focused on the antiviral action of Type I IFN, that form the host's first line of response. In the equations below, the cellular space fraction reduces (and the extracellular space fraction increases) as an outcome of these events. Parameters Φ and Ψ are the maximum hourly rates of FMDV-induced and IFN-mediated cell death respectively. We thus assume

$$\frac{\partial}{\partial t}(S_c) = - \underbrace{\Phi f(K) S_c}_{\text{FMDV-induced cell lysis}} - \underbrace{\Psi f_D(I_c, V_c) S_c}_{\text{IFN-mediated cell death}}, \tag{14}$$

$$\frac{\partial}{\partial t}(S_e) = \underbrace{\Phi f(K) S_c}_{\text{FMDV-induced cell lysis}} + \underbrace{\Psi f_D(I_c, V_c) S_c}_{\text{IFN-mediated cell death}}. \tag{15}$$

Intracellular resource, K, is depleted during FMDV replication while some resource is also removed from the system during cell death, hence

$$\begin{aligned} \frac{\partial}{\partial t}(K S_c) = &- \underbrace{\rho K h_R(E) g_G(E) f_R(I_c) V_c S_c}_{\text{loss of resource due to FMDV replication}} \\ &- \underbrace{\Phi f(K) K S_c}_{\text{loss of resource due to FMDV-induced cell lysis}} \\ &- \underbrace{\Psi f_D(I_c, V_c) K S_c}_{\text{loss of resource due to IFN-mediated cell death}}. \end{aligned} \tag{16}$$

Changes in intracellular, V_c, and extracellular, V_e, FMDV concentration are described in Eqs. (17) and (18), alongside IFN antiviral action. While FMDV-induced cell lysis leads to FMDV being released in the

extracellular space, it is assumed that during IFN-mediated death, FMDV and IFNs are deactivated and removed from the system, thus

$$\frac{\partial}{\partial t}(V_c S_c) = \underbrace{\xi\rho K h_R(E) g_G(E) f_R(I_c) V_c S_c}_{\text{FMDV replication}} + \underbrace{\mu g_G(E) h_U(E) f_U(I_c) V_e S_c}_{\text{FMDV uptake by cells}} - \underbrace{\gamma f_L(I_c) V_c S_c}_{\text{FMDV release by live cells}} - \underbrace{\Phi f(K) V_c S_c}_{\text{FMDV release due to FMDV-induced cell lysis}} - \underbrace{\Psi f_D(I_c, V_c) V_c S_c}_{\text{FMDV loss due to IFN-mediated cell death}}, \tag{17}$$

$$\frac{\partial}{\partial t}(V_e S_e) = -\underbrace{\mu g_G(E) h_U(E) f_U(I_c) V_e S_c}_{\text{FMDV uptake by cells}} + \underbrace{\gamma f_L(I_c) V_c S_c}_{\text{FMDV release by live cells}} + \underbrace{\Phi f(K) V_c S_c}_{\text{FMDV release due to FMDV-induced cell lysis}} + \underbrace{D_V \frac{\partial}{\partial x}\left(S_e \frac{\partial V_e}{\partial x}\right)}_{\text{FMDV diffusion}}. \tag{18}$$

We assume that FMDV infection triggers local production of IFN, within cells of the cellular column we examine. This is followed by IFN release to the extracelluar space, leading to IFN reaching neighbouring cells, binding to them and stimulating more IFN production. In unifected cells this is considered to be a low level production that serves in preparing them to respond to infection. In infected cells, IFN production is enhanced according to both IFN and viral load. Eqs. (19) and (20) describe these dynamics within cellular and extracellular space. Parameters ϵ_1 and ϵ_3 in the IFN production term define the level of production due to virus action alone and due to combined FMDV-IFN action respectively. Limitations to the level of production are imposed by parameters ϵ_2 and ϵ_4 which define the limits of FMDV-induced and IFN-induced production respectively, while θ is the hourly IFN production constant.

Beyond live cell release, IFNs are also released to the extracellular space because of FMDV-induced cell lysis. IFN-stimulated cell death is considered to lead to IFN deactivation, while some natural IFN decay occurs in both the cellular and extracellular space. We thus have

$$\frac{\partial}{\partial t}(I_c S_c) = \underbrace{\theta(I_c + \epsilon_1 V_c + \epsilon_3 I_c V_c) e^{(-\epsilon_4 I_c - \epsilon_2 V_c)} h_I(E) g_G(E) S_c}_{\text{IFN production}} + \underbrace{\mu_I h_{I_U}(E) g_G(E) I_e S_c}_{\text{IFN uptake by cells}} - \underbrace{\gamma_I I_c S_c}_{\text{IFN release by live cells}} - \underbrace{\Phi f(K) I_c S_c}_{\text{IFN release due to FMDV-induced cell lysis}} - \underbrace{\Psi f_D(I_c, V_c) I_c S_c}_{\text{IFN loss due to IFN-mediated cell death}} - \underbrace{\delta_{I_c} I_c S_c}_{\text{IFN decay in cells}}, \tag{19}$$

$$\frac{\partial}{\partial t}(I_e S_e) = -\underbrace{\mu_I h_{I_U}(E) g_G(E) I_e S_c}_{\text{IFN uptake by cells}} + \underbrace{\gamma_I I_c S_c}_{\text{IFN release by live cells}} + \underbrace{\Phi f(K) I_c S_c}_{\text{IFN release due to FMDV-induced cell lysis}} + \underbrace{D_I \frac{\partial}{\partial x}\left(S_e \frac{\partial I_e}{\partial x}\right)}_{\text{IFN diffusion}} - \underbrace{\delta_{I_e} I_e S_e}_{\text{IFN decay in extracellular space}}. \tag{20}$$

While Eqs. (14)–(18) have been based on [27], Eqs. (19) and (20) are newly introduced here. We note the model of [27] can be derived by setting $I_c = 0$.

2.3. Boundary and initial conditions

The initial conditions of the model describe the absence of IFN in the system and arrival of FMDV, hence at

$$t = 0 : S_c = \alpha, S_e = 1 - \alpha, K = K_0, V_c = 0,$$
$$V_e(x,0) = \begin{cases} V_0, & \text{for } x = e_p \\ 0, & \text{everywhere else.} \end{cases}, I_c(x,0) = 0, I_e(x,0) = 0.$$

representing healthy epithelial layers and the viral point of entry is at $x = e_p$.

The boundary conditions for E and V_c are the same as [27]. Only extracellular FMDV and IFN can escape from the system at $x = 0$ and is assumed permanently lost to the system; the fluxes of these being described using a Robin condition. At $x = 0$, the activator is fixed at concentration $E = E_0$. The spinus-granular interface is assumed inpenetrable, hence no flux conditions are imposed for all diffusible components. Here, we also account for the newly introduced extracellular IFN that are allowed to diffuse out of the basement membrane depending on a mass transfer coefficient, Q_I. The boundary conditions are thus,

$$x = 0 : E(0,t) = E_0, -D_V \frac{\partial V_e}{\partial x}(0,t) = -Q_V V_e(0,t), - D_I \frac{\partial I_e}{\partial x}(0,t) = -Q_I I_e(0,t)$$
$$x = L_P : -D_E \frac{\partial E}{\partial x}(L_P,t) = Q_E E(L_P,t), -D_V \frac{\partial V_e}{\partial x}(L_P,t) = Q_V V_e(L_P,t), -D_I \frac{\partial I_e}{\partial x}(L_P,t) = Q_I I_e(L_P,t)$$
$$x = L_T : \frac{\partial E}{\partial x}(L_T,t) = 0, \frac{\partial V_e}{\partial x}(L_T,t) = 0, \frac{\partial I_e}{\partial x}(L_T,t) = 0.$$

2.4. Numerical investigation

Eqs. (12)–(20) were non-dimensionalised and central difference approximations were used in place of spatial derivatives. The dimensionless equations are available in S1 Supplementary Information. The system of ordinary differential equations was solved numerically in Matlab using a variable order solver for stiff systems (based on Gear's method), namely ode15s (see Supplementary material).

2.5. Sensitivity analysis

Sensitivity analysis was undertaken on the model parameters to assess how sensitive the model outcomes (namely epithelial cell survival) are to changes in particular parameters. We performed a 100 replicates simulation with parameters sampled using a latin hypercube sampling (LHS) procedure [55]. This is well above the recommended lower limit for LHS, which is the number of uncertain parameters plus one [56]. Parameters that were selected from over several orders of magnitude were sampled logarithmically to avoid a bias towards larger magnitudes. Exponents m_1, m_2 and m_3 were chosen linearly over the range [1, 100].

3. Results

Numerical investigation of the model using the baseline parameter values (Table 2), shows complete cell survival in the DSP and some cell death in the tongue for the baseline of viral entry at the tissue surface for DSP and basement membrane for tongue (Figs. 2 and 3, Table S3.3 in Supplementary Information). It is important to remind the reader that the tongue cellular column is nearly ten times the size of that in the DSP, which means that the graphs of the tongue and the DSP are not spatially comparable. The minimum surviving epithelium, which is the minimum percentage of surviving epithelium across the epithelium thickness (x axis) 48 h after infection, is 100% in the DSP and 61% for the tongue (see Table S3.3 in Supplementary Information).

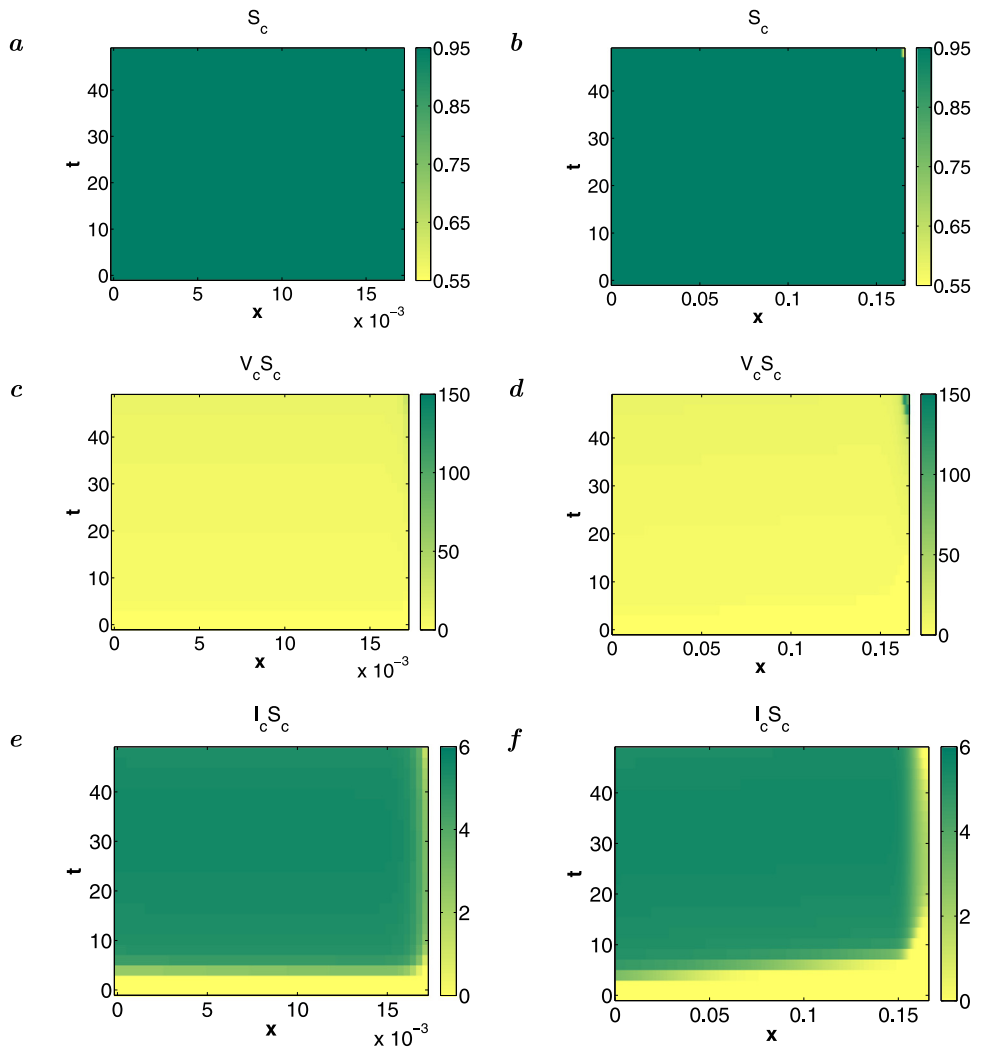

Fig. 2. Simulation results for cellular dynamics in DSP (left-hand column) and tongue (right-hand column) over a 48 h timescale. Epithelium surface used as the viral entry point for DSP and basement membrane as the viral entry point for tongue. (a), (b) Cellular space fraction, S_c, of DSP and tongue respectively. Cellular destruction is observed at the top right hand corner of the tongue graph. (c), (d) Intracellular virus load, V_cS_c, of DSP and tongue respectively measured in PFU/cm. (e), (f) Intracellular IFN load, I_cS_c, of DSP and tongue respectively measured in IU/cm.

Intracellular IFN loads peak early in both tissues (Figs. 2e and f) and remain at similar levels over time, though lower levels are observed close to the tissues' surface, with a large dip close to the tongue granular cell layer. Extracellular IFN loads on the other hand peak in the tongue at the same location, close to 48 h post infection (Fig. 3f). The tongue granular cell layer 48 h post infection, is the same spatiotemporal area in which the intracellular viral load increases and intracellular resource and the tongue space fraction decrease. This is because cell death results in release of IFN (i.e. a decrease in intracellular IFN) to the extracellular space (i.e. an increase in extracellular IFN).

One-way and multi-way sensitivity analysis results show the model to be highly sensitive to alterations of many parameters. These results are presented in S3 Supplementary Information in detail. However, probabilistic sensitivity analysis results using LHS show the model outcomes to be reliable within a range of values extending from half to double the default estimates of parameters μ, D_V, Q_V, V_0, μ_I, Ψ, δ_{I_e}, D_I, I_D and Q_I (Figs. 4 a and b). This remains the case when extending the range of parameter values to a fifth and five times their default estimates (Figs. 4 c and d).

In the one-way sensitivity analysis all parameters were explored for 10% differences to their values. Highly influential parameters were those for which this difference let to complete survival of both the tongue and DSP epithelia when tested one way and nearly complete destruction of one of the two tissues when tested the other way. Parameters of less influence were explored for values of two orders of magnitude difference. If within these bounds full survival or full tissue destruction was observed for both tongue and DSP, the maximum or minimum values for this to occur were identified. Where such variations were considered irrelevant, other values specific to the tested parameters were identified. The full results of this analysis are available in S3 Supplementary Information.

Altering the parameters defining the tongue's structure to resemble that of the DSP or altering its thickness to be equal to the that of the DSP led to full cell survival. The model shows high sensitivity to alterations of the maximal rate of FMDV replication, ξ, the rate of FMDV resource consumption, ρ, and the threshold concentration of IFN, I_R, that defines the suppression of FMDV replication. The maximal IFN production rate, θ, is also very influential alongside the rate of IFN release by cells, γ_I, and the site of infection.

Parameters of moderate influence are those regulating IFN-mediated cell death (IFN and FMDV threshold parameters I_D and V_D respectively); they influence results when combined, with I_D having some influence also on its own. Parameters ϵ_1 and ϵ_3 which regulate IFN production in response to FMDV concentration and to FMDV and IFN concentration combined respectively also impact results. Others include

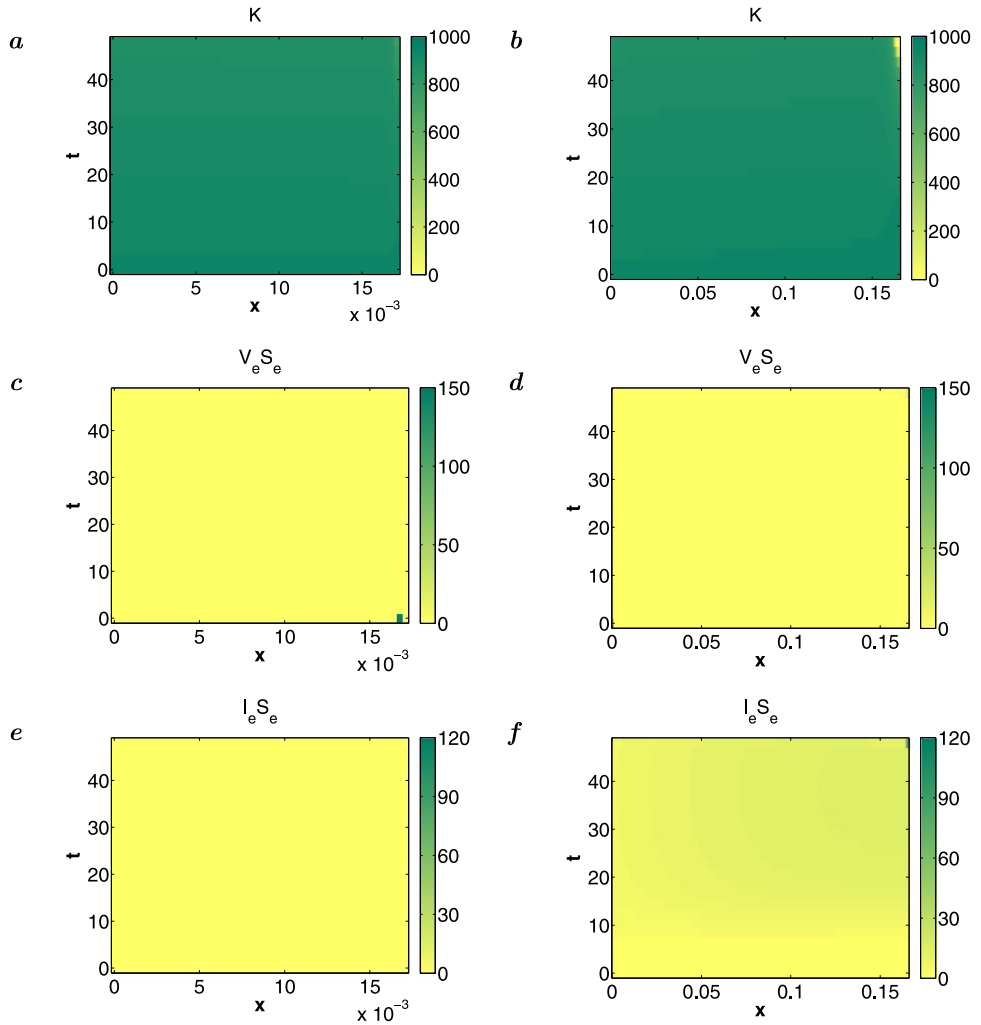

Fig. 3. Simulation results for extracellular dynamics in DSP (left-hand column) and tongue (right-hand column) over a 48 h timescale. Epithelium surface used as the viral entry point for DSP and basement membrane as the viral entry point for tongue. (a), (b) Intracellular resource, K, of DSP and tongue respectively, measured in cm^{-1}. (c), (d) Extracellular virus load, V_eS_e, of DSP and tongue respectively measured in PFU/cm. (e), (f) Extracellular IFN load, I_eS_e, of DSP and tongue respectively measured in IU/cm.

the intracellular natural IFN decay, δ_{I_c}, the rate of FMDV uptake by cells, μ, the FMDV diffusion coefficient, D_V, the FMDV concentration at the site of infection, V_0, the intracellular resource threshold, $K_{1/2}$, and the mass transfer coefficient of FMDV, Q_V. Combinations of the parameters expressing interlayer variability have also some influence (see Tables S3.4 and S3.5).

Parameters with minor or no influence on results are the rate of extracellular natural IFN decay, δ_{I_e}, the rate of IFN uptake by cells, μ_I, the IFN diffusion coefficient, D_I, and the IFN mass transfer coefficient, Q_I (see Table S3.2). The FMDV threshold parameter regulating IFN-mediated cell death, V_D, showed no impact for the tested values on its own.

4. Discussion

In this study we have explored the role of Type I IFN (IFN-α and IFN-β) as the first line of response to infection by FMDV. Our aim is to understand what drives the development of epithelial lesions in the tongue and their absence in the DSP, a difference which is based on observations of affected animals. We have investigated whether these different outcomes could be the result of differences in: (i) epithelium size and structure; (ii) initial site of infection; (iii) FMDV dynamics between tissues; (iv) FMDV dynamics in different layers of the same tissue; (v) IFN dynamics between tissues; (vi) IFN dynamics in different layers of the same tissue; (vii) interplay between FMDV and IFN between tissues. Our parameter values have been largely based on experimental data sourced from the published literature.

Our results show that epithelial tissue thickness and cell layer structure in combination with Type I IFN dynamics can explain the development of epithelial lesions in the tongue and their absence in the DSP for the baseline scenario of parameter estimates. This work has built on a previous model [27] which showed that epithelial tissue thickness and cell layer structure alone could not explain this behaviour. Here we have confirmed this result and we have also shown that Type I IFN dynamics, while very influential when the different epithelium thickness and cell layer structure of DSP and tonge is incorporated, alone cannot explain this behaviour either. It is the combined effect of the two factors that determines the development or absence of lesions.

The tongue is considered a secondary site of infection [6], and as such is thought to be normally infected at the basement membrane or potentially in spinous cells close to it [53]. While the former infection site was used in the baseline exploration, the model suggests that more cell death is observed if tongue is infected on the granular surface or a few cells deep. This is in agreement with our cellular column model [27] and suggests that lesions are deeper and more severe if infection occurs due to a cut or abrasion on the tongue surface. It also suggests that more pronounced lesions could occur if the

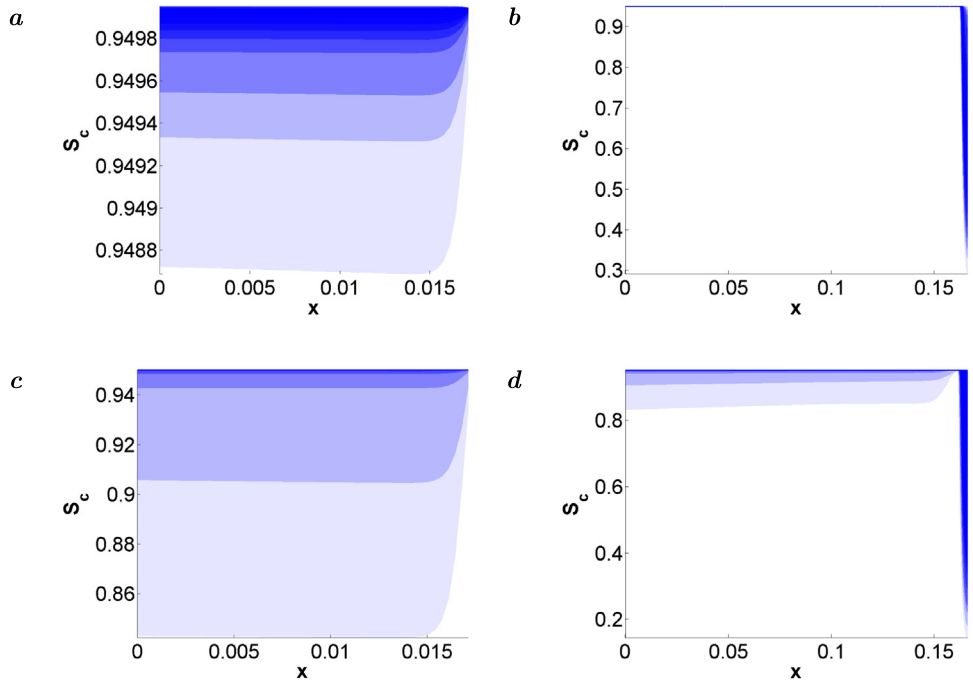

Fig. 4. LHS applied to the model with tested parameters ranging from 0.5 to 2 times their estimated values in (a) and (b) and from 0.2 to 5 times their estimated values in (c) and (d). These show the consistency of results in predicting total survival (in (a)) or nearly total survival (in (c)) of the cellular column in DSP and some destruction in tongue. In (a) and (b), S_c remains bounded above 0.948 for DSP, while S_c of tongue drops as low as 0.3 close to the granular layer. In (c) and (d) S_c remains bounded above 0.84 for DSP, while S_c of tongue drops below 0.2 close to the granular layer. The range of possible results is plotted in five percentile steps from 100 replicates, with eleven shades of blue starting form the median (darkest blue) and moving to lighter blue shades for each five percentiles on either direction. (a), (b) Results of DSP and tongue respectively. Parameters tested: μ, D_V, Q_V, V_0, μ_I, Ψ, δ_{I_c}, D_I, I_D and Q_I.

tongue is inoculated comparing with natural infection at the basement membrane.

We have highlighted the maximal rate of FMDV replication, ξ, and the rate of FMDV resource consumption, ρ, to be the most influential parameters in our previous model [27] and these remain highly influential here. Our study shows estimated viral replication rates can drive the different behaviour of the two tissues; different rates between tissues can increase cell death level differences. This emphasises the importance of estimating these parameters more precisely through purposely designed experimental work.

Through the current model we have also identified IFN-related parameters to have a large impact on the levels of cell death. The maximal rate of IFN production (θ) is in fact the most influential parameter in the model. It shows that different capacity for IFN production between tissues can explain the development or absence of lesions, though different behaviour between tissues can exist even if the capacity is the same. It is therefore crucial to understand further the dynamics of IFN production in response to infection, through a combination of experimental and mathematical work. This would provide us with more reliable parameter estimates, elucidate aspects of the mechanism of IFN production, and increase confidence in current findings.

We have also explored the role of FMDV replication suppression due to IFN action. Results show that higher suppression in the DSP could drive the absence of lesions in this tissue and their presence in the tongue epithelium. While such differences are not necessary to explain the different behaviour of the two tissues, this is another area where a mathematical approach alongside experimental work, could potentially enhance our understanding of this process and its role in FMDV-induced cell death.

Our results on the influence of viral replication, IFN production and IFN antiviral action on cell death are in agreement with that of Saenz et al. [22], who modelled influenza-IFN dynamics prior to the onset of adaptive immune response. Similarly to here, other models on dengue and avian influenza have also shown that suppression of viral replication by IFN can explain dynamics of virus-IFN interaction [15,21]. Howey et al. [9] investigated the role of both adaptive and immune response in FMDV infected cattle. In their model, however, FMDV persists in the circulation unless neutralised by antibodies while in our model it is depleted during cell lysis. This means that IFN production is not initiated when FMDV infects cells, as in our model, as this would lead to high production of IFN if FMDV is not neutralised fast enough. Instead, it is stimulated by virus-antibody complexes. While this may have the effect of the model fitting the IFN and FMDV curves of their experimental data, this would mean that innate immune response occurs after the onset of adaptive immune response which is not biologically realistic. Based on the above and the central role of adaptive immune response in the Howey et al. model, the findings of the two models are not comparable to each other.

The rate of IFN release by live cells is also important for cell death levels; an increased rate of release leads to more cell death, while different rates between the two tissues could drive the presence or absence of lesions. However, even with the current - *same* - rate for both tissues, different levels of cell death are observed. It is interesting to note that the rate of natural IFN decay in cells has a lesser – but still important – impact, with relatively small reductions in cellular IFN leading to more cell death in the tongue. It is therefore worth considering whether other biological mechanisms could be incorporated in this model. Saenz et al. for example highlight IFN clearance as a factor influencing cell death [22]. The possibility that cellular IFN are depleted during their antiviral action could be important in determining the levels of FMDV-induced cell death and it is important to explore this in future work.

Our results demonstrate how the initial dose of infection influences the level of cell death, which contradicts the findings of Saenz et al. [22]. Their model, however, includes virus clearance, which impacts cell death levels. In our work, virus can be de-activated only due to IFN-mediated cell death. Our model shows that an infectious dose of 1 pfu leads to extensive cell death in the tongue and negligible

death in the DSP. A dose of 10^{-2} pfu leads to both tissues remaining intact, while at 10^{2} pfu DSP remains intact but tongues exhibits even greater cell death. Howat et al. [8] suggest that doses of 10^{-2} pfu per cell lead to fast recovery of cell monolayers, with large doses leading to total cell destruction. They hypothesise that intermediate infection doses in vivo, will lead to patches of heavily infected epithelial cells becoming IFN producers that do not prevent further infection but rather stimulate immune response elsewhere. At what could be considered an intermediate dose based on Howat et al. our model suggests that IFN dynamics in combination with epithelial tissue thickness and cell layer structure could lead to very different outcomes in tissues. This suggests that the Howat et al. results in cell monolayers are more aligned with the FMDV-IFN dynamics in tongue where some destruction is observed with an intermediate dose and infected cells may have a role in stimulating the adaptive immune response, while in DSP cells are able to fight off the infection and escape cell death. It is worth noting that the models of Saenz et al. [22] and Howey et al. [9] are at the whole animal level so these may not be directly comparable with our within tissue model; the model of Howat et al. [8] of cell monolayers can be used for more direct comparisons.

While we have highlighted a number of mechanisms and parameters to be prioritised for future exploration, it is also interesting to note those that do not influence the different behaviour in DSP and tongue epithelia. In the model, the distribution of FMDV and IFN receptors, and the diffusion of FMDV and IFN within and out of the two epithielial tissues are shown not to determine the development of lesions in tongue and their absence in the DSP. The same applies for extracellular IFN decay.

Our exploration of potential interlayer variability shows that lower FMDV replication vulnerability in basal cells is more likely to result in lesions in the tongue than higher vulnerability. Furthermore, results are more consistent if IFN production competence is lower in basal cells, in comparison with if it is higher. These results are intuitive as there are far fewer basal cells, therefore changes to their dynamics cause less disruption to the baseline results. Our study shows that interlayer differences in IFN production, FMDV replication and FMDV-infected cell death vulnerability could determine the development or absence of lesions and they merit more through investigation.

5. Conclusions

Our study has shown that Type I IFN dynamics in combination with epithelial tissue thickness and structure are sufficient alone to determine the development of FMDV-induced lesions in the tongue epithelium and their absence in the DSP. FMDV replication, IFN production, IFN depletion in live cells (either due to release to the extracellular space or natural decay) and FMDV replication suppression can all determine the different behaviour in the two tissues. Interlayer variability in FMDV and IFN could also play a crucial role and requires more investigation.

We re-iterate the importance of interdisciplinary research in investigating within-host dynamics of infection, both for FMDV but also more widely in the field of infectious diseases. Mathematical modelling results are strengthened by bespoke experimental work seeking to fill a significant gap in relevant data.

Funding

This work was funded by the Biotechnology and Biological Sciences Research Council (BBSRC) [grant code: BBS/E/I/00001397].

Declaration of competing interest

None.

Acknowledgements

We are thankful to Bryan Charleston, Donald King, Marcus Tindall and Andrew Archer for their valuable comments.

Appendix A. Supplementary data

Supplementary material related to this article can be found online at https://doi.org/10.1016/j.mbs.2023.109052.

References

[1] M.M. Brierley, J. Kumaran, E.N. Fish, Biological actions of type I interferons, in: The Interferons, John Wiley & Sons, Ltd, 2006, pp. 164–206.
[2] J. Plachỳ, K.C. Weining, E. Kremmer, F. Puehler, K. Hala, B. Kaspers, P. Staeheli, Protective effects of type I and type II interferons toward rous sarcoma virus-induced tumors in chickens, Virol 256 (1) (1999) 85–91.
[3] U. Schultz, J. Köck, H.-J. Schlicht, P. Staeheli, Recombinant duck interferon: a new reagent for studying the mode of interferon action against hepatitis B virus, Virol 212 (2) (1995) 641–649.
[4] Z. Dinter, L. Philipson, An interferon produced by foot and mouth disease virus (FMDV) in calf kidney cells, in: Proceedings of the Society for Experimental Biology and Medicine. Society for Experimental Biology and Medicine, Vol. 109, No. 4, New York, NY, Royal Society of Medicine, 1962, pp. 893–897.
[5] G.N. Medina, F.D.-S. Segundo, C. Stenfeldt, J. Arzt, T. de los Santos, The different tactics of foot-and-mouth disease virus to evade innate immunity, Front. Microbiol. 9 (2018).
[6] S. Alexandersen, Z. Zhang, A.I. Donaldson, A.J.M. Garland, The pathogenesis and diagnosis of foot-and-mouth disease, J. Comp. Pathol. 129 (1) (2003) 1–36.
[7] C. Janeway, K. Murphy, P. Travers, M. Walport, Janeway's Immunobiology, seventh ed., Garland Science, 2008, pp. 94–95.
[8] T.J. Howat, C. Barreca, P. O'Hare, J.R. Gog, B.T. Grenfell, Modelling dynamics of the type I interferon response to in vitro viral infection, J. R. Soc. Interface 3 (10) (2006) 699–709.
[9] R. Howey, B. Bankowski, N. Juleff, N.J. Savill, D. Gibson, J. Fazakerley, B. Charleston, M.E. Woolhouse, Modelling the within-host dynamics of the foot-and-mouth disease virus in cattle, Epidemics 4 (2) (2012) 93–103.
[10] H.M. Dobrovolny, M.B. Reddy, M.A. Kamal, C.R. Rayner, C.A. Beauchemin, Assessing mathematical models of influenza infections using features of the immune response, PLoS One 8 (2) (2013) e57088.
[11] A. Boianelli, V.K. Nguyen, T. Ebensen, K. Schulze, E. Wilk, N. Sharma, S. Stegemann-Koniszewski, D. Bruder, F.R. Toapanta, C.A. Guzmán, et al., Modeling influenza virus infection: a roadmap for influenza research, Viruses 7 (10) (2015) 5274–5304.
[12] A.U. Neumann, N.P. Lam, H. Dahari, D.R. Gretch, T.E. Wiley, T.J. Layden, A.S. Perelson, Hepatitis C viral dynamics in vivo and the antiviral efficacy of interferon-α therapy, Science 282 (5386) (1998) 103–107.
[13] F.C. Bekkering, C. Stalgis, J.G. McHutchison, J.T. Brouwer, A.S. Perelson, Estimation of early hepatitis C viral clearance in patients receiving daily interferon and ribavirin therapy using a mathematical model, Hepatology 33 (2) (2001) 419–423.
[14] V. Venugopal, P. Padmanabhan, R. Raja, N.M. Dixit, Modelling how responsiveness to interferon improves interferon-free treatment of hepatitis C virus infection, PLoS Comput. Biol. 14 (7) (2018) e1006335.
[15] S.K. Sasmal, Y. Dong, Y. Takeuchi, Mathematical modeling on T-cell mediated adaptive immunity in primary dengue infections, J. Theoret. Biol. 429 (2017) 229–240.
[16] S. Patil, M. Fribourg, Y. Ge, M. Batish, S. Tyagi, F. Hayot, S.C. Sealfon, Single-cell analysis shows that paracrine signaling by first responder cells shapes the interferon-b response to viral infection, Sci. Signal 8 (2015).
[17] P. Baccam, C. Beauchemin, C.A. Macken, F.G. Hayden, A.S. Perelson, Kinetics of influenza A virus infection in humans, J. Virol. 80 (15) (2006) 7590–7599.
[18] B. Hancioglu, D. Swigon, G. Clermont, A dynamical model of human immune response to influenza A virus infection, J. Theoret. Biol. 246 (1) (2007) 70–86.
[19] E.A. Hernandez-Vargas, E. Wilk, L. Canini, F.R. Toapanta, S.C. Binder, A. Uvarovskii, T.M. Ross, C.A. Guzmán, A.S. Perelson, M. Meyer-Hermann, Effects of aging on influenza virus infection dynamics, J. Virol. 88 (8) (2014) 4123–4131.
[20] P. Cao, A.W. Yan, J.M. Heffernan, S. Petrie, R.G. Moss, L.A. Carolan, T.A. Guarnaccia, A. Kelso, I.G. Barr, J. McVernon, et al., Innate immunity and the inter-exposure interval determine the dynamics of secondary influenza virus infection and explain observed viral hierarchies, PLoS Comput. Biol. 11 (8) (2015) e1004334.
[21] X.-T. Xie, A. Yitbarek, S.U. Khan, S. Sharif, Z. Poljak, A.L. Greer, A within-host mathematical model of H9N2 avian influenza infection and type-I interferon response pathways in chickens, J. Theoret. Biol. 499 (2020) 110320.
[22] R.A. Saenz, M. Quinlivan, D. Elton, S. MacRae, A.S. Blunden, J.A. Mumford, J.M. Daly, P. Digard, A. Cullinane, B.T. Grenfell, et al., Dynamics of influenza virus infection and pathology, J. Virol. 84 (8) (2010) 3974–3983.

[23] S. Wang, M. Hao, Z. Pan, J. Lei, X. Zou, Data-driven multi-scale mathematical modeling of SARS-CoV-2 infection reveals heterogeneity among COVID-19 patients, PLoS Comput. Biol. 17 (2021) 1–28.
[24] S. Wang, Y. Pan, Q. Wang, H. Miao, A.N. Brown, L. Rong, Modeling the viral dynamics of SARS-CoV-2 infection, Math. Biosci. 328 (2020) 108438.
[25] M. Sadria, A.T. Layton, Modeling within-host SARS-CoV-2 infection dynamics and potential treatments, Viruses 13 (6) (2021) 1141.
[26] D. Schley, J. Ward, Z. Zhang, Modelling foot-and-mouth disease virus dynamics in oral epithelium to help identify the determinants of lysis, Bull. Math. Biol. 73 (2011) 1503–1529.
[27] K. Giorgakoudi, S. Gubbins, J. Ward, N. Juleff, Z. Zhang, D. Schley, Using mathematical modelling to explore hypotheses about the role of bovine epithelium structure in foot-and-mouth disease virus-induced cell lysis, PLoS One 10 (10) (2015) e0138571.
[28] M.J. Grubman, M.P. Moraes, F. Diaz-San Segundo, L. Pena, T. De Los Santos, Evading the host immune response: how foot-and-mouth disease virus has become an effective pathogen, FEMS Immunol. Med. Microbiol. 53 (1) (2008) 8–17.
[29] H. Masui, L. Castro, J. Mendelsohn, Consumption of EGF by A431 cells: evidence for receptor recycling, J. Cell Biol. 120 (1) (1993) 85–93, Available from: http://jcb.rupress.org/content/120/1/85.abstract.
[30] A. Buckley, J.M. Davidson, C.D. Kamerath, S.C. Woodward, Epidermal growth factor increases granulation tissue formation dose dependently, J. Surg. Res. 43 (4) (1987) 322–328.
[31] R.G. Thorne, S. Hrabetova, C. Nicholson, Diffusion of epidermal growth factor in rat brain extracellular space measured by integrative optical imaging, J. Neurophysiol. 92 (6) (2004) 3471–3481.
[32] P. Monaghan, H. Cook, P. Hawes, J. Simpson, F. Tomley, High-pressure freezing in the study of animal pathogens, J. Microsc. 212 (2003) 62–70.
[33] N. Tanaka, M. Sato, M.S. Lamphier, H. Nozawa, E. Oda, S. Noguchi, R.D. Schreiber, Y. Tsujimoto, T. Taniguchi, Type I interferons are essential mediators of apoptotic death in virally infected cells, Genes Cells 3 (1) (1998) 29–37.
[34] P. Monaghan, H. Cook, T. Jackson, M. Ryan, T. Wileman, The ultrastructure of the developing replication site in foot-and-mouth disease virus-infected BHK-38 cells, J. Gen. Virol. 85 (2004) 933–946.
[35] E. Baranowski, N. Sevilla, N. Verdaguer, C. Ruiz-Jarabo, E. Beck, E. Domingo, Multiple virulence determinants of foot-and-mouth disease virus in cell culture, J. Virol. 72 (1998) 6362–6372.
[36] S.S. Breesex Jr., R. Trautman, Free diffusion measured by biological assay in multilayered cells: II. Diffusion coefficient of foot-and-mouth disease virus determined by infectivity, Anal. Biochem. 1 (4–5) (1960) 307–316.
[37] E.M. Coccia, M. Severa, E. Giacomini, D. Monneron, M.E. Remoli, I. Julkunen, M. Cella, R. Lande, G. Uzé, Viral infection and Toll-like receptor agonists induce a differential expression of type I and λ interferons in human plasmacytoid and monocyte-derived dendritic cells, Eur. J. Immunol. 34 (3) (2004) 796–805.
[38] S. Feldman, M. Ferraro, H. Zheng, N. Patel, S. Gould-Fogerite, P. Fitzgerald-Bocarsly, Viral induction of low frequency interferon-α producing cells, Virol 204 (1) (1994) 1–7.
[39] Z. Yin, J. Dai, J. Deng, F. Sheikh, M. Natalia, T. Shih, A. Lewis-Antes, S.B. Amrute, U. Garrigues, S. Doyle, et al., Type III IFNs are produced by and stimulate human plasmacytoid dendritic cells, J. Immunol. 189 (6) (2012) 2735–2745.
[40] A. Branca, C.R. Faltynek, S.B. D'Alessandro, C. Baglioni, Interaction of interferon with cellular receptors. Internalization and degradation of cell-bound interferon, J. Biol. Chem. 257 (22) (1982) 13291–13296.
[41] D. Kalvakolanu, E. Borden, An overview of the interferon system: signal transduction and mechanisms of action, Cancer Invest. 14 (1) (1996) 25–53.
[42] G. Carpenter, L. King, S. Cohen, Epidermal growth factor stimulates phosphorylation in membrane preparations in vitro, Nature 276 (1978) 409–410.
[43] J. Filmus, M.N. Pollak, R. Cailleau, R.N. Buick, MDA-468, a human breast cancer cell line with a high number of epidermal growth factor (EGF) receptors, has an amplified EGF receptor gene and is growth inhibited by EGF, Biochem. Biophys. Res. Commun. 128 (2) (1985) 898–905.
[44] M.J. Grubman, B. Baxt, Foot-and-mouth disease, Clin. Microbiol. Rev. 17 (2) (2004) 465–493.
[45] Y. Tan, J.A. Armstrong, M. Ho, Intracellular interferon: kinetics of formation and release, Virol 45 (3) (1971) 837–840.
[46] L. Perino, E. Short Jr., L. Burge, D. Winter, R. Fulton, Interferon and 2',5'-oligo(A) synthetase activities in serum and blood mononuclear leukocytes of cattle after injection of bovine interferon-alpha 1, Am. J. Vet. Res. 51 (6) (1990) 886–892.
[47] X. Ao, J.A. Stenken, Microdialysis sampling of cytokines, Methods 38 (4) (2006) 331–341.
[48] reprokine, Human epithelial growth factor recombinant, 2012, Available from: http://www.reprokine.com/ID2847_Human_Epidermal_Growth_Factor_Recombinant. (Accessed 2 August 2012).
[49] J.M. Taylor, S. Cohen, W.M. Mitchell, Epidermal growth factor: high and low molecular weight forms, Proc. Natl. Acad. Sci. USA 67 (1970) 164–171.
[50] S. Yonehara, M. Yonehara-Takahashi, A. Ishii, Binding of human interferon α to cells of different sensitivities: studies with internally radiolabeled interferon retaining full biological activity, J. Virol. 45 (3) (1983) 1168–1171.
[51] H. Shimizu, Shimizu's Textbook of Dermatology, Hokkaido University Press, 2007, http://www.derm-hokudai.jp/shimizu-dermatology/ch01/index.html. (Accessed 2 March 2013).
[52] P. Monaghan, S. Gold, J. Simpson, Z. Zhang, P.H. Weinreb, S.M. Violette, S. Alexandersen, T. Jackson, The $\alpha v\beta 6$ integrin receptor for foot-and-mouth disease virus is expressed constitutively on the epithelial cells targeted in cattle, J. Gen. Virol. 86 (10) (2005) 2769–2780.
[53] P. Monaghan, J. Simpson, C. Murphy, S. Durand, M. Quan, S. Alexandersen, Use of confocal immunofluorescence microscopy to localize viral nonstructural proteins and potential sites of replication in pigs experimentally infected with foot-and-mouth disease virus, J. Virol. 79 (10) (2005) 6410–6418.
[54] R.E. Randall, S. Goodbourn, Interferons and viruses: an interplay between induction, signalling, antiviral responses and virus countermeasures, J. Gen. Virol. 89 (1) (2008) 1–47.
[55] M.D. McKay, R.J. Beckman, W.J. Conover, Comparison of three methods for selecting values of input variables in the analysis of output from a computer code, Technometrics 21 (2) (1979) 239–245.
[56] S. Blower, H. Dowlatabadi, Sensitivity and uncertainty analysis of complex models of disease transmission: an HIV model, as an example, Int. Stat. Rev. 62 (1994) 229–243.